Gain/Phase Imbalance-Minimization Techniques for LINC Transmitters

Xuejun Zhang, *Student Member, IEEE*, Lawrence E. Larson, *Fellow, IEEE*, Peter M. Asbeck, *Fellow, IEEE*, and Peter Nanawa

***Abstract*—Two simple calibration schemes for the correction of the path imbalance in a linear amplification with nonlinear components (LINC) transmitter have been demonstrated. In the foreground algorithm, a baseband digital signal processor (DSP) evaluates the gain and phase imbalance with a set of calibration signals, while in the background algorithm, the imbalance is characterized by exchanging the two LINC vector components. In both cases, the compensation of the path imbalance is accomplished within the DSP by introducing a predistortion term. A prototype LINC system has been tested for CDMA IS-95 baseband input, and −38 and −35-dBc adjacent channel interference were achieved for the foreground and background schemes, respectively. The quadrature errors of the in-phase/quadrature modulators set a limit on the overall performance of both algorithms.**

***Index Terms*—Amplifier linearization, LINC, mobile communications, outphasing power amplifiers, RF power amplifiers.**

I. Introduction

THE outphased power amplifier concept dates back to the early 1930's as an approach for the simultaneous realization of high-efficiency and high-linearity amplification [1]. It has been revived recently for wireless communication applications under the rubric of linear amplification with nonlinear components (LINC) [2]; many recent papers have developed the concept further [3]–[19], including a variation called CALLUM [8], [9]. The LINC concept takes an envelope modulated bandpass waveform and resolves it into two out-phased constant envelope signals, which are applied to highly efficient—and highly nonlinear—power amplifiers, whose outputs are summed. The advantage of this approach is that each amplifier can be operated in a very power-efficient mode, and yet the final output can be highly linear and free of intermodulation—a key consideration for bandwidth efficient wireless communications.

One of the major disadvantages of this technique is the extremely tight tolerance on the matching of the two amplifier paths to achieve acceptably small out-of-band rejection. The out-of-band spectrum, created by the incomplete cancellation of the quadrature signal, strongly depends upon the modulation schemes. This problem has been analyzed by a number of authors, and the typical requirements for most practical applications are approximately 0.1–0.5 dB in gain matching or 0.4°–2° in-phase matching. This is nearly impossible to achieve in most practical situations, and several attempts have been made to correct for the errors. A "phase-only" correction was proposed in [14]. A simplex search algorithm was proposed in [15] to correct for both gain and phase errors. This algorithm requires a long data sequence for the measurement of the out-of-band emission, which sets a lower limit on the calibration time of around 1–2 s. A direct search method was proposed in [16] to correct the gain imbalance, as well as the consequent phase imbalance due to AM–PM transition. A method was presented in [17], in which path imbalance and quadrature imbalance are characterized by a few RF power measurements at different locations. All of these techniques may suffer from limitations of effectiveness and practicality.

We have proposed a calibration scheme, in which the evaluation of path imbalance (both gain and phase) is based on the measurement on a set of simple down-converted and low-pass filtered calibration signals [18]. In spite of its simplicity and effectiveness, the application of this technique is limited since the calibration is not transparent to data transmission. An alternative calibration scheme has been developed in [19], which operates continuously in background during regular data transmission, thus requiring no interruption of the transmitted signal for calibration. In this approach, the gain and phase imbalance are characterized by exchanging two LINC vector components and controlling a down-conversion loop. Henceforth, the two calibration schemes will be referred to as "foreground" and "background" algorithms, respectively.

This paper begins with an introduction to the principle of the LINC transmitter. Two calibration techniques are then described and the theoretical analysis is presented. Emphasis is placed on the background calibration scheme. The foreground algorithm is briefly reviewed and the detailed analysis and simulation results can be found in [18]. The experimental results of both calibration schemes are discussed, and finally conclusions are given.

II. Principle of LINC Transmitter

The basic principle of LINC is to represent arbitrary bandpass signals by means of two out-phased constant envelope signals; these two signals are then amplified separately with a pair of highly nonlinear and power-efficient amplifiers, and finally recombined through a passive combiner, as shown in Fig. 1. The separation of the bandpass signal is accomplished by the signal

Manuscript received March 29, 2001; revised August 21, 2001. This work was supported by the Army Research Office Multiuniversity Research Initiative Program Digital Communication Devices Based on Nonlinear Dynamics and Chaos, and by the University of California at San Diego Center for Wireless Communications and its supporting member companies.

X. Zhang, L. E. Larson, and P. M. Asbeck are with the Center for Wireless Communications, University of California at San Diego, La Jolla, CA 92093 USA.

P. Nanawa is with the Center for Wireless Communications, University of California at San Diego, La Jolla, CA 92093 USA and is also with the Single Chip Systems Corporation, San Diego, CA 92127 USA.

Publisher Item Identifier S 0018-9480(01)10767-2.

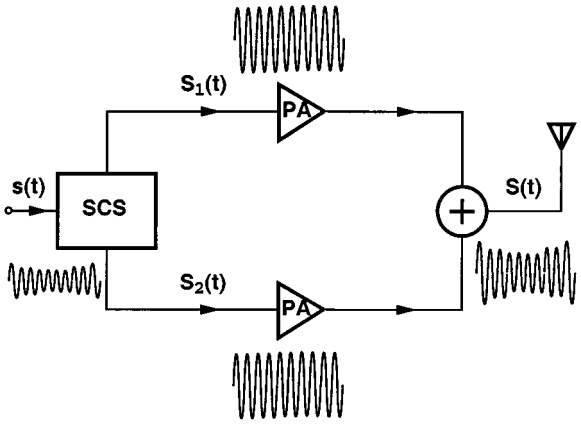

Fig. 1. Simplified LINC block diagram.

component separator (SCS). The detailed analysis of signal separation can be found in [3]–[5], and a brief mathematical description is given below.

A complex representation of the band-limited source signal can be written as

$$s(t) = a(t)e^{j\theta(t)}; \qquad 0 \le a(t) \le V_m. \tag{1}$$

This signal is split by the SCS into two signals with modulated phase and constant amplitude

$$S_1(t) = s(t) - e(t) = V_m e^{j[\theta(t)-\psi(t)]} \tag{2a}$$

$$S_2(t) = s(t) + e(t) = V_m e^{j[\theta(t)+\psi(t)]} \tag{2b}$$

where

$$\psi(t) = \cos^{-1}\left[\frac{a(t)}{V_m}\right] \tag{3}$$

and the quadrature signal $e(t)$ is defined by

$$e(t) = js(t)\sqrt{\frac{V_m^2}{a^2(t)} - 1}. \tag{4}$$

The two signals are then amplified individually and sent to the power combiner. If two amplifier paths are perfectly matched, such that their gain and phase characteristics are exactly the same, the in-phase signal components add together and the out-of-phase components cancel each other; the resultant signal is the desired amplified replica of the original signal. In practice, however, this condition is difficult to achieve. In contrast to the narrow-band source signal $s(t)$, the spectrum of quadrature signal $e(t)$ extends far into adjacent channels [15], and the incomplete cancellation of wide-band components leaves a residue in adjacent channels, hence, introducing adjacent channel interference (ACI).

III. Foreground Calibration Algorithm

The improved LINC system with foreground calibration makes use of the standard of amplitude and phase produced by the digital signal processor (DSP) to calibrate the amplifiers through a feedback loop, as is illustrated in Fig. 2. Note that two balanced modulators are employed to translate the baseband signal to the desired carrier frequency. While the DSP generates the calibration signals, a small portion of the power is withdrawn by a directional coupler. This signal is then down-converted, low-pass filtered, A/D converted, and finally sent back to the DSP. The DSP extracts the gain and phase imbalance, and eliminates the error effects by introducing a correction term. As a matter of fact, the DSP modulates and filters the original baseband signal, and compensates the gain and phase imbalance—the SCS functions to simultaneously generate the data signal and predistortion. Suppose that the gain and phase imbalance of the lower amplifier with respect to the upper one are $\Delta G/G_0$ and $\Delta\phi$, respectively, the LINC output signal will be

$$S(t) = G_0 V_m \cos\left[\omega_c t + \theta(t) - \psi(t) + \phi_0\right] + \left(1 + \frac{\Delta G}{G_0}\right) G_0 V_m \cdot \cos\left[\omega_c t + \theta(t) + \psi(t) + \phi_0 + \Delta\phi\right] \tag{5}$$

where G_0 and ϕ_0 are the amplifier gain and phase delay, respectively. The signal after low-pass filtering can be expressed as

$$S_{\mathrm{LPF}} = \frac{1}{2} G_L V_m \cos\left[\theta(t) - \psi(t) + \phi_L\right] + \frac{1}{2}\left(1 + \frac{\Delta G}{G_0}\right) G_L V_m \cdot \cos\left[\theta(t) + \psi(t) + \phi_L + \Delta\phi\right] \tag{6}$$

where G_L is the effective gain of the entire loop, and ϕ_L includes phase delay of the calibration loop and phase shift introduced by downconversion mixer.

The correction algorithm [18] consists of several steps. First, we set the amplitude of the input baseband signal to the maximum allowable level of the SCS, i.e., $a(t) = V_m$. We then set $\theta(t) = 0$, which means $I_1 = I_2 = V_m$ and $Q_1 = Q_2 = 0$. After eliminating higher order terms, the result from (6) is

$$S_0 \approx G_L' V_m \cos\left(\phi_L + \frac{1}{2}\Delta\phi\right) \tag{7}$$

where $G_L' = (1 + \Delta G/2G_0)G_L$. This result S_0 is stored in the DSP. Similarly, by setting $\theta(t) = \pi/2$ and keeping $a(t) = V_m$, corresponding to $I_1 = I_2 = 0$ and $Q_1 = Q_2 = V_m$, (6) becomes

$$S_p \approx -G_L' V_m \sin\left(\phi_L + \frac{1}{2}\Delta\phi\right). \tag{8}$$

We then set the amplitude of the input baseband signal to zero, i.e., $a(t) = 0$. As before, we set $\theta(t) = 0$, i.e., $I_1 = I_2 = 0$, $Q_1 = -V_m$, and $Q_2 = V_m$, to obtain S_a, and set $\theta(t) = \pi/2$, i.e., $I_1 = V_m$, $I_2 = -V_m$, and $Q_1 = Q_2 = 0$, to obtain S_b. From (6)–(8), we may write S_a and S_b in matrix from as

$$\begin{pmatrix} S_a \\ S_b \end{pmatrix} \approx -\frac{1}{2}\begin{pmatrix} -S_p & S_0 \\ S_0 & S_p \end{pmatrix}\begin{pmatrix} \Delta G/G_0 \\ \Delta\phi \end{pmatrix}. \tag{9}$$

Solving (9) for $\Delta G/G_0$ and $\Delta\phi$ yields

$$\frac{\Delta G}{G_0} \approx \frac{1}{P_L}\left(S_p S_a - S_0 S_b\right) \tag{10a}$$

$$\Delta\phi \approx -\frac{1}{P_L}\left(S_0 S_a + S_p S_b\right) \tag{10b}$$

where

$$P_L = \frac{1}{2} G_L^2 V_m^2 \tag{11}$$

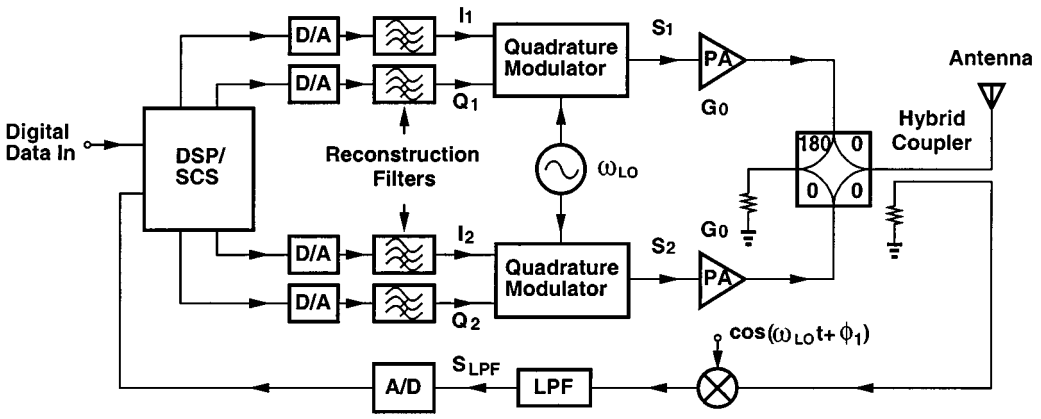

Fig. 2. LINC transmitter with foreground calibration loop.

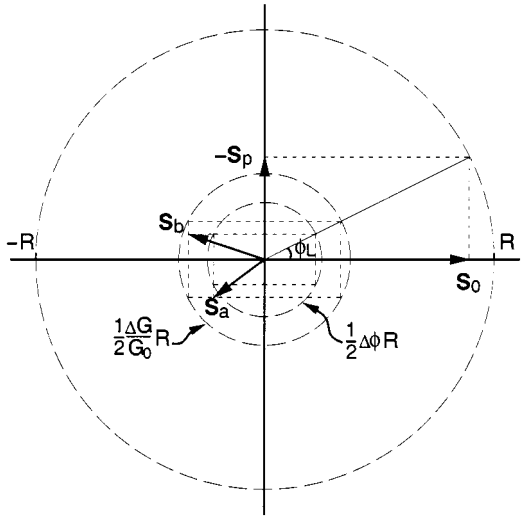

Fig. 3. Relationship between path imbalance and calibration signals. $R = G_L V_m$.

stands for the "average" power level normalized to a 1-Ω characteristic impedance during calibration, and can be computed by

$$P_L \approx \frac{1}{2}\left(S_0^2 + S_p^2\right). \tag{12}$$

Equation (9) indicates that the gain and phase imbalance are solely determined by S_0, S_p, S_a, and S_b. The relationships among them, as well as P_L and ϕ_L, are best illustrated in Fig. 3 in the case of small gain and phase imbalance, where S_a and S_b are the linear combinations of S_0 and S_p scaled by the gain and phase imbalance.

The approximations in (7)–(9) give rise to a certain amount of estimation error for the measurement of the gain and phase imbalance. Note, however, that the estimation error reduces to zero as gain and phase imbalance decrease to zero. This implies that these approximations are effective in the sense that the estimate and compensation of gain and phase imbalance are iterative; with several iterations, the gain and phase imbalance are able to converge to an acceptable low level [18]. Besides, since the accuracy of P_L is not critical in determining path imbalance, the evaluation of this quantity only need to be done once, further simplifying the algorithm.

IV. Background Calibration Algorithm

The application of the foreground calibration scheme is limited due to the fact that a specific time slot is required for calibration, and the calibration and data transmission cannot operate simultaneously. By comparison, the background calibration is transparent to regular data transmission. The key—if we look back at (5)—is that four different combinations of $a(t)$ and $\theta(t)$ are necessary to determine the gain and phase imbalance [18]. Now, instead of generating a set of calibration signals, the background scheme simply makes use of information data itself as a kind of calibration signal. The four combinations are realized by mixing the LINC output with two LINC signal vectors, and by exchanging these two vectors in the two amplifier branches. Also, instead of measurement of calibration signals, the DSP/SCS searches for four extreme signal values in these cases. As will be demonstrated, these four quantities completely determine the gain and phase imbalance.

A. Algorithm Theory

As in the foreground algorithm, the background calibration scheme characterizes the gain and phase imbalance through a feedback loop. As shown in Fig. 4, a small portion of the LINC output is coupled into the feedback loop and down-converted by a mixer. The mixed signal is then low-pass filtered, D/A converted, and sent back to the DSP/SCS, which abstracts the gain and phase imbalance information. Comparing it to Fig. 2 for the foreground algorithm, the local oscillator (LO) branch S_3 of the mixer is different. The baseband digital circuit controls the third branch signal such that S_3 connects to either the upper or lower amplifier branches. In each case, the DSP regularly exchanges two LINC vectors S_1 and S_2 in two amplifier branches back and forth. Before the DSP exchanges S_1/S_2, the LINC output is the same as (5). When the DSP exchanges the two LINC vectors S_1/S_2, it becomes

$$S(t) = G_0 V_m \cos\left[\omega_c t + \theta(t) + \psi(t) + \phi_0\right] + \left(1 + \frac{\Delta G}{G_0}\right) G_0 V_m \cdot \cos\left[\omega_c t + \theta(t) - \psi(t) + \phi_0 + \Delta\phi\right]. \tag{13}$$

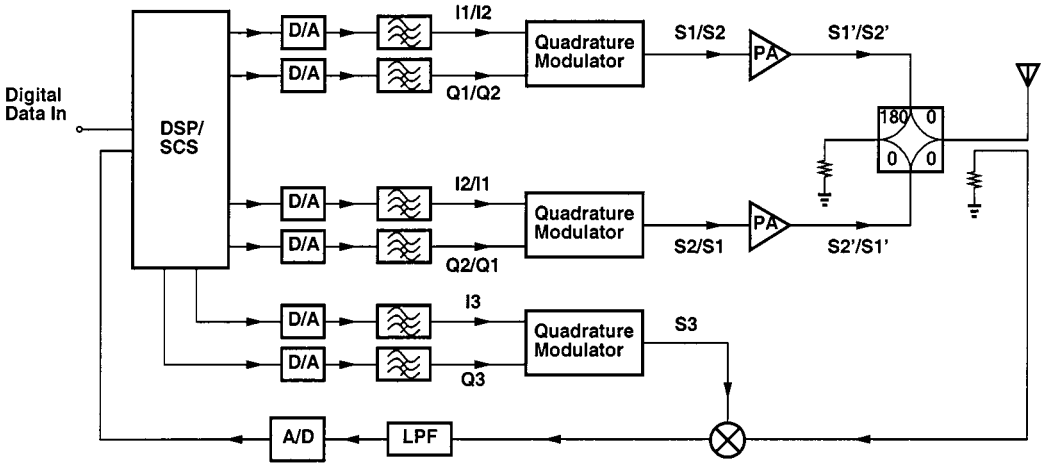

Fig. 4. LINC transmitter with background calibration loop.

We may combine (5) and (13) and rewrite it as follows:

$$S(t) = G_0 V_m \cos\left[\omega_c t + \theta(t) \mp \psi(t) + \phi_0\right] + \left(1 + \frac{\Delta G}{G_0}\right) G_0 V_m \cdot \cos\left[\omega_c t + \theta(t) \pm \psi(t) + \phi_0 + \Delta\phi\right] \quad (14)$$

where "$\mp$" and "$\pm$" are the consequences of exchanging two vectors S_1/S_2. Note that, as long as the path balance is maintained, the exchange between S_1/S_2 makes little difference to the LINC output signal. When S_3 connects to the upper branch, called state "A," we have

$$S_{3A}(t) = V_3 \cos\left[\omega_c t + \theta(t) \mp \psi(t) + \phi_3\right] \quad (15)$$

where V_3 stands for the signal amplitude of the mixer branch, and ϕ_3 is the phase delay. The downconversion mixer multiplies the LINC output (14) with (15). After low-pass filtering, we obtain

$$S_{\mathrm{LPF}} = \frac{1}{2} G_L V_m \cos\phi_L + \frac{1}{2}\left(1 + \frac{\Delta G}{G_0}\right) G_L V_m \cdot \cos\left[\pm 2\psi(t) + \phi_L + \Delta\phi\right] \quad (16)$$

where G_L is the loop gain and ϕ_L consists of the loop phase delay and the phase shift introduced by the downconversion mixer. The only time variable in (16) is $\psi(t)$, and (16) is actually a time-varying sinusoidal signal modulated by the baseband signal amplitude and offset by a dc constant. Unlike the foreground algorithm, there is no way for us to know when to measure a specific signal. However, it is obvious that the dc offset and the amplitude of this sinusoidal function carry information of the gain and phase imbalance and they can be extracted by determining the two extreme cases—the maximum and minimum signal values. This function is accomplished by the baseband DSP/SCS. Particularly, the DSP searches the extreme signal values before and after the exchange of the two LINC vectors. By comparing these four measured values, the maxima and minima values are then determined. The band-limited characteristics of the baseband input implies that the amplitude $a(t)$ has a large variation with time. As stated previously, $0 \le a(t) \le V_m$ or $0^\circ \le \psi(t) \le 90^\circ$, hence, we have

$$-180^\circ \le \pm 2\psi(t) \le 180^\circ. \quad (17)$$

The above expression guarantees that the maximum and minimum signal values can be found, i.e.,

$$\max_A = \frac{1}{2} G_L V_m \cos\phi_L + \frac{1}{2}\left(1 + \frac{\Delta G}{G_0}\right) G_L V_m \quad (18a)$$

$$\min_A = \frac{1}{2} G_L V_m \cos\phi_L - \frac{1}{2}\left(1 + \frac{\Delta G}{G_0}\right) G_L V_m. \quad (18b)$$

The exchanging of S_1/S_2 may cause an overshoot of the output envelope to the DSP because of the phase discontinuity in the S_3 branch before/after exchanging and the transient effect of the low-pass filter (LPF), which, in turn, degrades the measurement accuracy of maxima/minima. This error effect can be minimized by exchanging S_1/S_2 when these two vectors are close to each other, i.e., $a(t) \approx V_m$, and/or possibly hold the DSP/SCS for a short period of time when exchanging S_1/S_2, to allow the output of the LPF to reach steady state. Now, two quantities are obtained by combining the following maxima and minima:

$$S_{A+} = \max_A + \min_A = G_L V_m \cos\phi_L \quad (19a)$$

$$S_{A-} = \max_A - \min_A = \left(1 + \frac{\Delta G}{G_0}\right) G_L V_m. \quad (19b)$$

Similar procedures applied to the state "B," when the DSP switches S_3 to the lower amplifier branch. Specifically, S_3 connects to the lower branch, and it is then mixed with the LINC output. After the LPF, we obtain

$$S_{\mathrm{LPF}} = \frac{1}{2}\left(1 + \frac{\Delta G}{G_0}\right) G_L V_m \cos(\phi_L + \Delta\phi) + \frac{1}{2} G_L V_m \cos\left[\mp 2\psi(t) + \phi_L\right]. \quad (20)$$

Again, it is a time-varying sinusoidal signal, but this time its amplitude and dc offset change slightly. The DSP searches the maximum and minimum signal values, and by combining these two extreme values, S_{B+} and S_{B-} can be computed as follows:

$$S_{B+} = \left(1 + \frac{\Delta G}{G_0}\right) G_L V_m \cos(\phi_L + \Delta\phi) \quad (21a)$$

$$S_{B-} = G_L V_m. \quad (21b)$$

Comparing (19b) and (21b), we immediately obtain the gain imbalance

$$\frac{\Delta G}{G_0} = \frac{S_{A-}}{S_{B-}} - 1. \tag{22}$$

The determination of phase imbalance is a little bit more involved since this quantity is resolved from $\cos(\phi_L + \Delta\phi)$ and $\cos\phi_L$, which are calculated by the two ratios of (19) and (21). Considering ϕ_L as a small quantity, the resolution of $\Delta\phi$ from $\cos(\phi_L + \Delta\phi)$ strongly depends upon ϕ_L. This situation occurs due to the finite word-length representation of the voltage waveform by ADC and, hence, limited SNR in the calibration loop

$$\Delta\phi_{\text{resolution}} = \left|\frac{d(\cos\phi_L)}{d\phi}\right| \tag{23a}$$

$$= |\sin\phi_L|. \tag{23b}$$

The maximum resolution happens as $|\sin\phi_L| = 1$, and the resolution reduces sinusoidally to zero as $\sin\phi_L = 0$. This optimum condition can be achieved by monitoring the ratio $\cos\phi_L = S_{a+}/S_{b-}$ and introducing a proper phase shift in the S_3 branch such that $S_{a+}/S_{b-} \approx 0$. As a fairly rough estimation, we have

$$\Delta\phi \approx \pm\left[\cos\phi_L - \cos(\phi_L + \Delta\phi)\right] \tag{24a}$$

$$\approx \pm\left(\frac{S_{A+}}{S_{B-}} - \frac{S_{B+}}{S_{A-}}\right) \tag{24b}$$

where the "±" sign is determined by ϕ_L. The approximation of the above equation is valid by assuming $\sin\phi_L \approx \pm 1$. However, in a similar manner, as P_L in the foreground calibration, $\sin\phi_L$ only scales the measured phase imbalance. Hence, the accurate determination of $\sin\phi_L$ is not critical and unnecessary, and (24) is effective in an iterative sense, even if ϕ_L cannot be well controlled. The estimation error is given by

$$\frac{\Delta\phi_{\text{err}}}{\Delta\phi_{\text{act}}} = \frac{\Delta\phi_{\text{est}} - \Delta\phi_{\text{act}}}{\Delta\phi_{\text{act}}} = \frac{\cos\phi_L - \cos(\phi_L + \Delta\phi) - \Delta\phi}{\Delta\phi} \tag{25}$$

and shown in Fig. 5. The estimation error would be less than 25% for a 90°±40° on ϕ_L with respect to the optimum point, and a 0.2°–20° variation on phase imbalance. This suggests that the correction of the phase imbalance can be iteratively accomplished. With a few iterations, the phase imbalance will be reduced to and arbitrarily low level, as long as we set a proper allowable phase imbalance.

B. Effects of I/Q Modulator Quadrature Errors

In practice, the quadrature errors of the in-phase/quadrature (I/Q) modulators degrades the accurate determination of the path imbalance and the algorithm convergence. The situation is more complicated than that in the foreground case since now there are three I/Q modulator branches. For simplicity, we will assume that all the quadrature errors are equal, i.e., $g_{1,2,3} = \delta_{1,2,3} = \delta$. This will simplify the calculations and the final

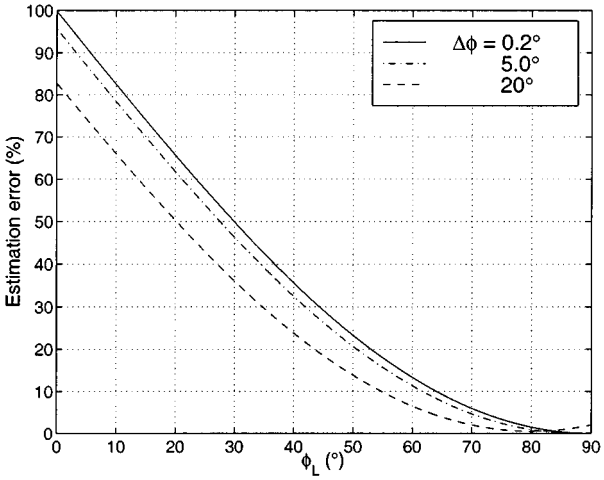

Fig. 5. Estimation error with respect to ϕ_L.

results still provide general directions. By using the same definitions of quadrature errors as in the previous section, the two LINC vectors are

$$S_1(t) = G_0 V_m \cos(\omega_c t + \phi_0)\cos\left[\theta(t) \mp \psi(t)\right] - (1+\delta)G_0 V_m \sin(\omega_c t + \phi_0 + \delta)\sin\left[\theta(t) \mp \psi(t)\right] \tag{26a}$$

$$S_2(t) = \left(1 + \frac{\Delta G}{G_0}\right)G_0 V_m \cos(\omega_c t + \phi_0 + \Delta\phi) \cdot \cos\left[\theta(t) \pm \psi(t)\right] - (1+\delta)\left(1 + \frac{\Delta G}{G_0}\right)G_0 V_m \cdot \sin(\omega_c t + \phi_0 + \Delta\phi + \delta)\sin\left[\theta(t) \pm \psi(t)\right]. \tag{26b}$$

These two signals are then combined and mixed with S_3. The resulting expression after low-pass filtering is rather lengthy. Here, we only give the simplified expressions after dropping off higher order terms. For state "A," we have

$$S_{LPF} \approx \frac{1}{2}(1+\delta)G_L V_m \cos\phi_L + \frac{1}{2}\left(1 + \frac{\Delta G}{G_0}\right)(1+\delta)G_L V_m \cdot \cos\left[\pm 2\psi(t) + \phi_L + \Delta\phi\right] + \sqrt{2}\delta G_L V_m \cos\phi_L \cdot \sin[2\theta(t) \mp \psi(t)]\cos\left[\mp\psi(t) - 45^\circ\right]. \tag{27}$$

The measured dc offset and signal amplitude are computed in the worst cases

$$S_{A+} = (1+\delta)G_L V_m \cos\phi_L \tag{28a}$$

$$S_{A-} = (1+\delta)\left(1 + \frac{\Delta G}{G_0}\right)G_L V_m + 2\sqrt{2}\delta G_L V_m \cos\phi_L. \tag{28b}$$

Similarly, we have the following simplified expression for state "B":

$$S_{\text{LPF}} \approx \frac{1}{2}\left(1 + \frac{\Delta G}{G_0}\right)(1+\delta)G_L V_m \cos(\phi_L + \Delta\phi) + \frac{1}{2}(1+\delta)G_L V_m \cos\left[\pm 2\psi(t) - \phi_L)\right] + \sqrt{2}\delta G_L V_m \cos\phi_L \sin\left[2\theta(t) \pm \phi_L - 45^\circ\right] \cdot \sin\left[\pm\psi(t)\right]. \tag{29}$$

S_{B+} and S_{B-} are given by

$$S_{B+} = \left(1 + \frac{\Delta G}{G_0}\right)(1+\delta) G_L V_m \cos(\phi_L + \Delta\phi) \quad (30a)$$

$$S_{B-} = (1+\delta) G_L V_m + 2\sqrt{2}\delta G_L V_m \cos\phi_L. \quad (30b)$$

The gain imbalance is calculated according to (22)

$$\left(\frac{\Delta G}{G_0}\right)_{\text{est}} = \frac{S_{A-}}{S_{B-}} - 1 \approx \left(\frac{\Delta G}{G_0}\right)_{\text{act}} \quad (31)$$

and the phase imbalance can be calculated by

$$\Delta\phi_{\text{est}} = \pm\left(\frac{S_{B+}}{S_{A-}} - \frac{S_{A+}}{S_{B-}}\right) \approx \Delta\phi_{\text{act}}\left(1 - 2\sqrt{2}\delta\cos\phi_L\right). \quad (32)$$

Apparently for the first-order approximation, the quadrature errors of the I/Q modulator will not affect the measurement of the gain imbalance, while the measurement error of the phase imbalance has the same order of the quadrature errors. As we know, $\cos\phi_L$ is kept close to zero for optimum estimation on the phase imbalance. This reduces the effects of quadrature errors, and the quadrature errors may not be a major limitation on the performance of the algorithm convergence.

C. More Practical Considerations

The characterization of the gain and phase imbalance takes advantage of the time-varying characteristics of the baseband input signal. In other words, if the baseband input signal has constant amplitude, this calibration scheme will fail. However, there is no reason to use an outphasing amplifier system to amplify such a constant amplitude signal. In reality, the baseband input is a band-limited signal and, thus, has a large amplitude variation. Equation (16) is rewritten here for convenience as follows:

$$S_{\text{LPF}} = G_L V_m \cos\phi_L + \left(1 + \frac{\Delta G}{G_0}\right) G_L V_m \cdot \cos\left[\pm 2\psi(t) + \phi_L + \Delta\phi\right]. \quad (33)$$

Assume that the optimum condition applies, i.e., $\phi_L = \pm 90°$. To guarantee the DSP finds the maxima and minima, the amplitude variation of the baseband signal has to satisfy the following expression:

$$\frac{\max[a(t)]}{\min[a(t)]} > \sqrt{2}. \quad (34)$$

This situation is illustrated in Fig. 6, in which at least $\pm 90°$ variation on $\pm 2\psi(t)$ are required in order that the cosine function passes through its maxima and minima from the optimum point. Thus, (34) is the minimum requirement and is applicable to most practical applications. In case the S_3 branch is not well controlled, the variation of the signal amplitude has to increase accordingly to accommodate the deviation from the optimum point.

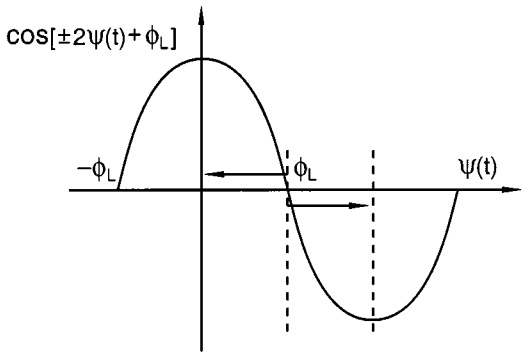

Fig. 6. Minimum requirement on the amplitude variation of the baseband signal.

In practice, the dc offset of the mixer, the LPF, and the ADC add to the measured signal values as a constant background and degrade the measurement accuracy. Note, however, that the dc offset will not affect the accuracy of the measured gain imbalance since it cancels out in S_{A-} and S_{B-}. There are a few options to determine this offset and subtract it from S_{A+} and S_{B+}. For example, in a similar manner to the foreground calibration algorithm, the dc offset can be determined by adding an extra degree of freedom to the measurement, such as reversing the phase in the S_3 branch, or changing the attenuation of the calibration loop with a variable attenuator. Probably the simplest way is to disable the downconversion mixer driving signal, and take the measurement on the background dc offset directly.

The minimization of the bit length of the A/D converter is also an important concern in practice in order to reduce the computation load of the DSP. The quantization error of the A/D converter degrades the measurement accuracy and the algorithm convergence. For a $(B+1)$-bit A/D converter, we have

$$\Delta = \frac{X_m}{2^B} \quad (35)$$

where Δ and X_m are the step size and full-scale level of the A/D converter, respectively. According to (16)

$$X_m = G_L V_m / 2. \quad (36)$$

As we know, the quantization error is bounded by $\Delta/2$, hence, we have the worst-case estimation errors

$$(S_{A,\,B\pm})_{\text{est}} = (S_{A,\,B\pm})_{\text{act}} \pm \Delta \quad (37)$$

and the estimation errors of the gain and phase imbalance are bounded by

$$\left(\frac{\Delta G}{G_0}\right)_{\text{est}} \approx \left(\frac{\Delta G}{G_0}\right)_{\text{act}} \pm \frac{2\Delta}{G_L V_m} \quad (38a)$$

$$\Delta\phi_{\text{est}} \approx \Delta\phi_{\text{act}} \pm \frac{4\Delta}{G_L V_m}. \quad (38b)$$

As it turns out, the word length of the A/D converter should satisfy

$$B+1=2-\frac{\log_{10}\delta}{\log_{10}2} \tag{39}$$

where δ is the preset maximum allowable gain or phase imbalance. As an example, for the allowable imbalance better than 2° for phase or 0.3 dB for gain, a 7-bit word-length representation would be adequate, which corresponds to around -40 dB ACI for CDMA IS-95. This is easily achievable with modern A/D converter technology.

V. Measured Results and Discussion

A LINC prototype system has been constructed to demonstrate the two calibration schemes. In this system, a personal computer, two arbitrary waveform generators, and a digital oscilloscope are used to simulate the function of the DSP/SCS. The waveform generators and oscilloscope are industry standard architecture (ISA) cards plugged into the computer's expansion slots. Each waveform generator is capable of two channel outputs. By configuring them as master/slave, two waveform generators are synchronized to generate four-channel outputs. An external trigger source is used to trigger the waveform generators and digital oscilloscope.

The power amplifier has nominal 29 dBm of 1-dB compression point and 27-dB gain. The upper amplifier operates at the gain compressed by 2 dB as a fairly nonlinear amplifier. In order to adjust the power of the bottom branch to compensate the gain imbalance, the bottom amplifier operates 3 dB backed off from the 1-dB compression point in the linear region. The maximum capable output power of this system is 31 dBm.

Since very limited memory size is available in the waveform generator, short filtered pseudonoise (PN) sequences are used as the baseband sources. The baseband filters were designed to meet CDMA IS-95 specifications. The waveform generators simply repeat the filtered PN sequences—no spurs will be generated. The chip rate is 1.23 MHz and the carrier frequency is 850 MHz.

A. Foreground Algorithm

The foreground calibration experiment starts with a calibration in which two arbitrary waveform generators generate four-channel synchronized calibration signals. At the same time, a snapshot is taken by a digital oscilloscope. The gain and phase imbalance are then evaluated and stored. At the end of each iteration, the DSP/SCS recalculate the imbalance. These steps are repeated until the measured imbalance is under certain low level, and then the waveform generators load in and generate the CDMA IS-95 baseband signals with compensation of the path imbalance.

Fig. 7(a) shows the calibration signal waveform I_1 and Q_1. I_2 and Q_2 are not shown here; their waveforms are a time-shifted version of Q_1 and I_1. The dashed lines indicate when the DSP/SCS takes the samples of the signal after low-pass filtering. Between dashed lines are the transitions that can be carefully designed to minimize out-of-band spurs during calibration. The transient effect of the LPF is not crucial in this case. Note

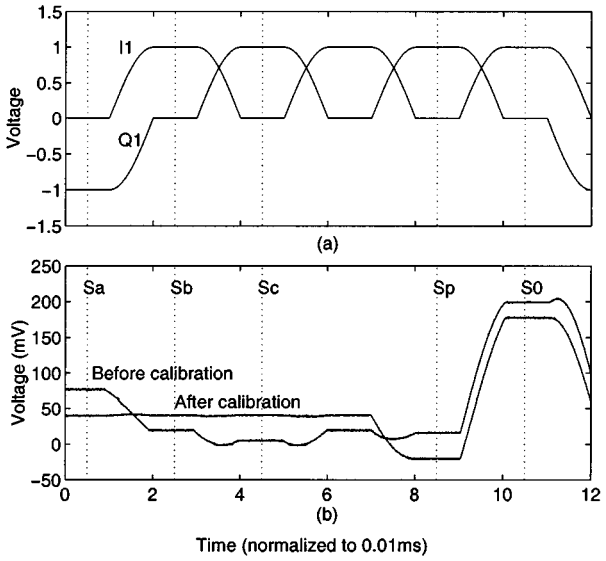

Fig. 7. (a) Calibration signal waveforms I_1 and Q_1. (b) Measured values before/after calibration from digital oscilloscope.

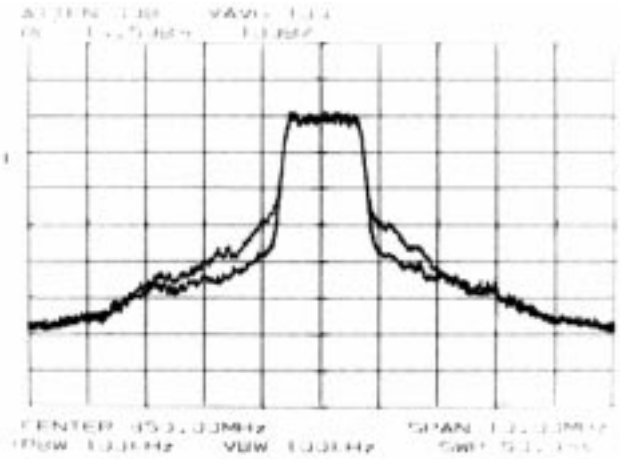

Fig. 8. Measured LINC output spectra for CDMA IS-95 with and without calibration using the foreground correction scheme.

that an extra calibration signal S_c is added, which is used to determine the dc offset of the LPF and A/D converter. This offset adds to the measured values and degrades the measurement accuracy and iteration convergence. S_c can be chosen to be a signal which is 180° out-of-phase with any of the four calibration signals; in this example, we choose to set $a(t)=0$ and $\theta(t)=\pi$, i.e., $I_1=I_2=0$, $Q_1=V_m$, and $Q_2=-V_m$. From (6), the dc offset is easily determined by

$$V_{\text{offset}}=\frac{S_a+S_c}{2} \tag{40}$$

and can then be subtracted from measured values. The calibration was accomplished within 2–3 iterations. Each iteration took 0.12 ms, and can be further reduced if necessary.

Fig. 7(b) compares signals taken by a digital oscilloscope before and after calibration. From (9), we immediately see that, for a perfectly matched system, S_a, S_b, and S_c should remain zero—the constant dc offset in this case, which is consistent

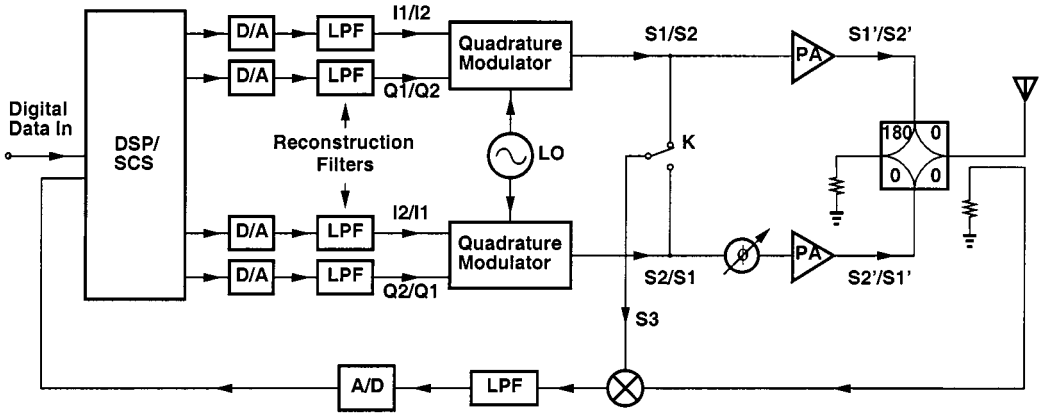

Fig. 9. LINC transmitter with alternative background calibration loop.

with the experiment. As we know, CDMA IS-95 mobile terminals transmit signal in bursts, which implies that calibration could be taken very shortly before real data transmission, with two zero-RF power-level signals (S_a and S_b) followed by two full-RF power-level signals (S_0 and S_p) at the beginning of every few bursts.

Fig. 8 displays the output power spectrum of the LINC transmitter. Without correction, the ACI is around -27 dB, while with correction, the out-of-band spectrum is suppressed efficiently below -38 dBc. Here, ACI is defined as the ratio of the peak spectral density of the out-of-band residue to the peak spectral density of the modulation. The measured gain and phase imbalance prior to calibration are 0.5 dB and 12°, respectively. The relatively large phase imbalance is mainly contributed by the mismatching of the two power amplifiers since the upper amplifier operates in saturation and the bottom one operates linearly. Considering that each modulator in our system has nominal 2° phase error and 0.3-dB gain error, and the calibrated gain and phase imbalance are [18]

$$\frac{\Delta G}{G_0} = (g_1 - g_2)\sin^2\phi + (\delta_1 - \delta_2)\sin\phi\cos\phi \quad (41a)$$

$$\Delta\phi = (\delta_1 - \delta_2)\cos^2\phi + (g_1 - g_2)\sin\phi\cos\phi \quad (41b)$$

then the -38-dBc ACI is reasonable. In our experiment, this system is able to achieve -41-dBc ACI without the power amplifiers. Here, g and δ are the amplitude and phase error of the I/Q modulators, respectively. There is little we can do to minimize the effects of quadrature errors of the I/Q modulators since these errors are random in nature. In fact, the performance of the foreground and background algorithms is limited by the quadrature errors. Fortunately, highly accurate quadrature modulators are routinely available for up- and down-conversion applications [20].

B. Background Algorithm

The background calibration in Fig. 4 requires an extra RF branch compared to foreground calibration, including two D/A converters, two reconstruction filters, and one I/Q modulator. This added complexity becomes more complicated considering the matching among these three branches. Though three RF branches are involved in background calibration, only two different LINC signal components are taken to calibrate the system—S_1 and S_2. Thus, instead of adding one extra waveform generator, in our experiment, we use an RF switch that connects to either of two LINC RF branches to construct the S_3 branch. This is considered as an alternative implementation approach of the background calibration scheme, as illustrated in Fig. 9. The baseband DSP controls the RF switch "K" to connect the upper or bottom amplifier branch, and this coupled RF signal is mixed with the LINC output. A preamp may be needed to drive the downconversion mixer if necessary.

Since the RF switch couples S_1/S_2 to the downconversion mixer, the signal amplitude and phase difference between the states "A" and "B" in the S_3 branch is directly transformed into the mixer output and create discrepancy between the measurement and actual values of the path imbalance. This is not true for the amplitude difference since the mixer can operate in saturation, and its output is not sensitive to the relatively small amplitude variation of the LO driving signal. Moreover, though the RF switch branch requires careful phase matching, detailed analysis shows that the phase difference between the two switch states affect only the measured phase imbalance, and not gain imbalance. Suppose that the phase mismatch between states "A" and "B" is δ, it can be shown that the measured phase imbalance is given by

$$\Delta\phi_{\text{est}} = \Delta\phi_{\text{act}} - \delta. \quad (42)$$

Hence, the final phase imbalance converges to δ.

Fig. 10 displays a snapshot taken by digital oscilloscope during state "B." The abrupt transition in the middle of the graph corresponds to the moment of exchange between S_1 and S_2. The quantity ϕ_L, in this case, was kept around 70°. If $\phi_L = 90°$, the waveforms before and after exchanging will look antisymmetric with respect to the transition point. The transition point becomes less obvious and finally indistinguishable as ϕ_L approximates to zero. The digital oscilloscope recorded a few little overshoots, and this effect was minimized by data averaging. A short period of data (20 μs) is also displayed as an inset in Fig. 10 to illustrate the rapid variation of the low-pass filtered signal. Theoretically each iteration of calibration could be accomplished in the order of tens of microseconds.

The output power spectra of the LINC transmitter are showed in Fig. 11. Without correction, the ACI is around -28 dB, while

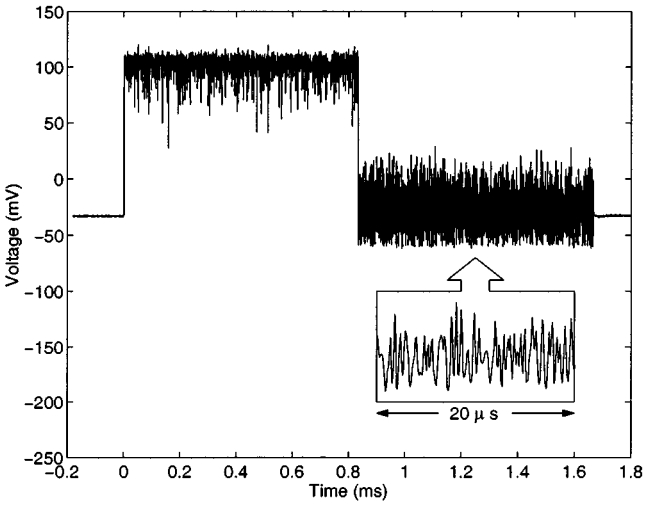

Fig. 10. Low-pass filtered signal taken by a digital oscilloscope during background calibration.

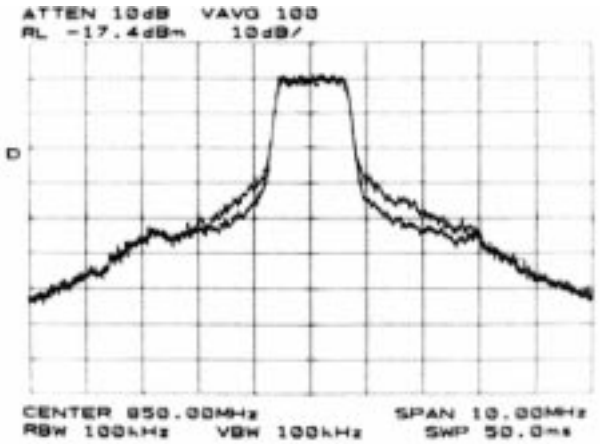

Fig. 11. Measured LINC output spectra with background calibration for CDMA IS-95 with and without calibration.

with correction, the out-of-band spectrum is suppressed below −35 dBc. The measured gain and phase imbalance prior to calibration are 0.6 dB and 8°, respectively. The reason that the background calibration achieved less than the foreground calibration is due to the matching of the reconstruction filters since the background scheme involves exchanging between S_1/S_2. It was found in our experiment that the output spectrum is sensitive to the matching of filters, and could introduce as large as 3-dB difference in ACI.

VI. Conclusion

Two novel calibration schemes have been analyzed for the correction of the gain and phase imbalance in a LINC transmitter. The foreground algorithm simply characterizes the path imbalance through a set of calibration signals, while the background one characterizes the path imbalance by exchanging the two LINC vector components and managing the downconversion loop. The background scheme has the advantage of being transparent to regular data transmission and, hence, its application is independent of communication standards. A prototype LINC system has been constructed to demonstrate the two calibration schemes for CDMA IS-95, and −38 and −35 dBc ACI were achieved, respectively, compared to −28 dBc without calibration. The theoretical analysis and experimental results demonstrate that both calibration schemes are sufficient to suppress the out-of-band emission for wireless communications.

References

[1] H. Chireix, "High power outphasing modulation," *Proc. IRE*, vol. 23, pp. 1370–1392, Nov. 1935.
[2] D. C. Cox, "Linear amplification with nonlinear components," *IEEE Trans. Commun.*, vol. COM-23, pp. 1942–1945, Dec. 1974.
[3] L. Couch and J. L. Walker, "A VHF LINC amplifier," in *Proc. IEEE Southeastcon'82*, Destin, FL, pp. 122–125.
[4] S. A. Hetzel, A. Bateman, and J. P. McGeehan, "LINC transmitter," *Electron. Lett.*, vol. 27, no. 10, pp. 844–846, May 1991.
[5] F. Casadevall and J. J. Olmos, "On the behavior of the LINC transmitter," in *Proc. 40th IEEE Veh. Technol. Conf.*, Orlando, FL, May 6–9, 1990, pp. 29–34.
[6] F. H. Raab, "Efficiency of outphasing RF power-amplifier systems," *IEEE Trans. Commun.*, vol. COM-33, pp. 1094–1099, Oct. 1985.
[7] L. Sundstrom, "The effect of quantization in a digital signal component separator for LINC transmitters," *IEEE Trans. Veh. Technol.*, vol. 45, pp. 346–352, May 1996.
[8] K. Y. Chan, A. Bateman, and M. Li, "Analysis and realization of the LINC transmitter using the combined analogue locked loop universal modulator CALLUM," in *Proc. IEEE 44th Veh. Technol. Conf.*, vol. 1, Stockholm, Sweden, June 8–10, 1994, pp. 484–488.
[9] K. Y. Chan and A. Bateman, "Linear modulators based on RF synthesis: Realization and analysis," *IEEE Trans. Veh. Technol.*, vol. 42, pp. 321–333, June 1995.
[10] D. J. Jennings and J. P. McGeehan, "A high-efficiency RF transmitter using VCO-derived synthesis: CALLUM," *IEEE Trans. Veh. Technol.*, vol. 47, pp. 715–721, June 1999.
[11] L. Sundstrom and M. Johansson, "Effect of modulation scheme on LINC transmitter power efficiency," *Electron. Lett.*, vol. 30, no. 20, pp. 1643–1645, Sept. 1994.
[12] L. Sundstrom, "Effects of reconstruction filters and sampling rate for a digital signal component separator on LINC transmitter performance," *Electron. Lett.*, vol. 31, no. 14, pp. 1124–1125, July 1995.
[13] ——, "Spectral sensitivity of LINC transmitters to quadrature modulator misalignments," *IEEE Trans. Veh. Technol.*, vol. 49, pp. 1474–1487, July 2000.
[14] S. Tomisato, K. Chiba, and K. Murota, "Phase error free LINC modulator," *Electron. Lett.*, vol. 25, no. 9, pp. 576–577, Apr. 1989.
[15] L. Sundstrom, "Automatic adjustment of gain and phase imbalances in LINC transmitters," *Electron. Lett.*, vol. 31, no. 3, pp. 155–156, Feb. 1995.
[16] S. Ampem-Darko and H. S. Al-Raweshidy, "Gain/phase imbalance cancellation technique in LINC transmitters," *Electron. Lett.*, vol. 34, no. 22, pp. 2093–2094, Oct. 1998.
[17] S. A. Olson and R. E. Stengel, "LINC imbalance correction using baseband preconditioning," in *IEEE Radio Wireless Conf.*, Denver, CO, Aug. 1999, pp. 179–182.
[18] X. Zhang and L. E. Larson, "Gain and phase error free LINC transmitter," *IEEE Trans. Veh. Technol.*, vol. 49, pp. 1986–1994, Sept. 2000.
[19] X. Zhang, L. E. Larson, and P. M. Asbeck, "Calibration scheme for LINC transmitter," *Electron. Lett.*, vol. 37, no. 5, pp. 317–318, Mar. 2001.
[20] I. A. Koullias, J. H. Havens, I. G. Post, and P. E. Bronner, "A 900-MHz transceiver chip set for dual-mode cellular radio mobile terminals," in *ISSCC Tech. Dig.*, Feb. 1993, pp. 140–141.

Xuejun Zhang (S'01) received the B.S. degree in semiconductor physics from Peking University, Beijing, China, in 1991, the M.S. degree in electrooptics from National University of Singapore, Singapore, in 1997, and is currently working toward the Ph.D. degree in electrical engineering at the University of California at San Diego, La Jolla.

From 1991 to 1992, he was with Southwestern Computing Center, Sichuan, China. From 1992 to 1995, he was with the Institute of Applied Electronics, Sichuan, China, where he was involved in various research projects including laser optics, optical diagnostic system, nonlinear optics, and optical materials. His current research interests include RF power amplifiers and power-amplifier linearization techniques for wireless communications.

Lawrence E. Larson (S'83–M'86–SM'90–F'00) received the B.S. degree in electrical engineering and the M.Eng. degree from Cornell University, Ithaca, NY, in 1979 and 1980, respectively, and the Ph.D. degree in electrical engineering from the University of California at Los Angeles, in 1986.

In 1980, he joined the Hughes Research Laboratories, Malibu, CA, where he directed work on high-frequency InP, GaAs, and silicon integrated-circuit development for a variety of radar and communications applications, as well as microelectromechanical system (MEMS)-based circuits for RF and microwave applications. He was also the Assistant Program Manager of the Hughes/Defense Advanced Research Projects Agency (DARPA) Monolithic-Microwave Integrated-Circuit (MIMIC) Program from 1992 to 1994. From 1994 to 1996, he was with Hughes Network Systems, Germantown, MD, where he directed the development of RF integrated circuits for wireless communications applications. In 1996, he joined the faculty of the University of California at San Diego (UCSD), La Jolla, where he is the Inaugural Holder of the Communications Industry Chair. He holds 21 U.S. patents.

Dr. Larson is a member of Sigma Xi and Eta Kappa Nu. He was corecipient of the 1996 Lawrence A. Hyland Patent Award of Hughes Electronics for his work on low-noise millimeter-wave high electron-mobility transistors (HEMTs).

Peter M. Asbeck (M'75–SM'97–F'00) received the B.S. and Ph.D. degrees in electrical engineering from the Massachusetts Institute of Technology (MIT), Cambridge, in 1969 and in 1975, respectively.

He was with the Sarnoff Research Center, Princeton, NJ, and at the Philips Laboratory, Briarcliff Manor, NY, where he was involved in the areas of quantum electronics and GaAlAs/GaAs laser physics and applications. In 1978, he joined the Rockwell International Science Center, where he was involved in the development of high-speed devices and circuits using III–V compounds and heterojunctions. He pioneered the effort to develop HBTs based on GaAlAs/GaAs and InAlAs/InGaAs materials, and has contributed widely in the areas of physics, fabrication, and applications of these devices. In 1991, he joined the University of California at San Diego (UCSD), La Jolla, as Professor in the Department of Electrical and Computer Engineering. His research interests are in development of high-speed heterojunction transistors and opto-electronic devices, and their circuit applications.

Dr. Asbeck is a distinguished lecturer of the IEEE Electron Device Society and of the IEEE Microwave Theory and Techniques Society (IEEE MTT-S). He is a member of the Department of Defense Advisory Group on Electron Devices. He was the general chairman of the 1996 Device Research Conference, and the chairman of the 1999 IEEE Topical Workshop on Power Amplifiers for Wireless Communications.

Peter Nanawa received the B.S. degree in bioengineering from the University of California at San Diego, La Jolla, in 1998, and is currently working toward the M.S. degree in electrical engineering at the University of California at San Diego, La Jolla.

He is currently an RF/Analog Application-Specific Integrated-Circuit (ASIC) Designer at the Single Chip Systems Corporation, San Diego, CA.